# KOH-activated multi-walled carbon nanotubes as platinum supports for oxygen reduction reaction

Chaoxiong He [a], Shuqin Song [a,*], Jinchao Liu [a], Vasiliki Maragou [b], Panagiotis Tsiakaras [b,**]

[a] State Key Laboratory of Optoelectronic Materials and Technologies, School of Physics and Engineering, Sun Yat-sen University, Guangzhou 510275, China
[b] Department of Mechanical Engineering, School of Engineering, University of Thessaly, Pedion Areos, 38834 Volos, Greece

## ABSTRACT

In the present investigation, multi-walled carbon nanotubes (MWCNTs) thermally treated by KOH were adopted as the platinum supporting material for the oxygen reduction reaction electrocatalysts. FTIR and Raman spectra were used to investigate the surface state of MWCNTs treated by KOH at different temperatures (700, 800, and 900 °C) and showed MWCNTs can be successfully functionalized. The structural properties of KOH-activated MWCNTs supported Pt were determined by X-ray diffraction (XRD) and transmission electron microscopy (TEM), and their electrochemical performance was evaluated by the aid of cyclic voltammetry (CV) and rotating disk electrode (RDE) voltammetry. According to the experimental findings of the present work, the surrface of MWCNTs can be successfully functionalized with oxygen-containing groups after activation by KOH, favoring the good dispersion of Pt nanoparticles with narrow size distribution. The as-prepared Pt catalysts supported on KOH treated MWCNTs at higher temperature, possess higher electrochemical surface area and exhibit desirable activity towards oxygen reduction reaction (ORR). More precisely, it has been found that the electrochemical active area of Pt/MWCNTs-900 is approximately two times higher than that of Pt/MWCNTs. It can be concluded that KOH activation is an effective way to decorate MWCNTs' surface with oxygen-containing groups and bigger surface area, which makes them more suitable as electrocatalyst support materials.

© 2010 Elsevier B.V. All rights reserved.

## 1. Introduction

Proton exchange membrane fuel cells (PEMFCs) systems are a type fuel cell developed for transport applications as well as for small-scale stationary and portable fuel cell applications [1]. Their advantages include the environmental friendly and low temperature operation, as well as quick start-up and shut-down procedures. In the specific operation system, hydrogen is considered as the preferred fuel in virtue of its high activity and its environmental benignity. Along with the PEMFCs development, low molecular alcohols (especially methanol and ethanol) are also directly fed into the anode as the fuel because of the easy handle of liquid fuel and their high power density [2]. Whatever the case may be, Pt or Pt-based binary or ternary catalysts are still the well-known catalyst materials providing desirable performance for electrode reactions. To make full use of Pt and reduce Pt usage, Pt-based catalysts are usually dispersed on carbon supports with high surface area. However, with the coexistence of Pt, the corrosion of carbon supports

will be accelerated especially at the cathode, and in this way, the Pt nanoparticles will be aggregated into a big one, leading to the activity loss of Pt [3,4].

On the other hand, with the development level of PEMFCs system, the total Pt storage in the world would be depleted if each car, which is powered by a 100 kW fuel cell stack, needs 100 g Pt [5]. One and a half billion cars will need 150,000 ton of Pt, which is far more than the estimated Pt resources in the world (28,000 ton) [3], let alone the other wide application of Pt in the area of catalysis, jewellery and so on. Based on this, the challenging issue of the high catalyst cost resulting from the exclusive adoption of Pt or Pt-based catalysts must be addressed, and in this way to promote the commercial viability of PEMFCs. A fundamental solution in this direction is the adoption of low Pt catalysts for fuel cell reactions. For this purpose, recently, many efforts have been oriented towards the development of new oxygen reduction reaction (ORR) electrocatalysts with lower Pt loadings supported on carbon nanotubes, focusing at the same time on the synergistic effect between catalyst and support.

Carbon nanotubes (CNTs) are a kind of one-dimensional carbon materials, which is nano level in the radial size and micron level in the axial size. For the use as catalyst support, the typical characteristics of CNTs correspond to 10–50 nm for the outer diameter, and 3–15 nm for the inner diameter, while the length ranges from 10 to

---

50 μm [6]. The tubular structure provides CNTs with unique properties including high surface area, excellent electronic conductivity, and high chemical stability, making them suitable to be exploited as support materials in heterogeneous catalysis and fuel cells [6–10], gas storage [11–13], field emission display [14] and supercapacitors [15].

CNTs supported Pt or Pt-based catalysts have also shown better electrocatalytic behavior than the conventional carbon materials in direct alcohol fuel cells [7,10]. Both single walled carbon nanotubes (SWCNTs) and multi-walled carbon nanotubes (MWCNTs) have the ability to promote electron-transfer reactions when used as an electrode material in electrochemical reactions [16]. However, the production cost of MWCNTs is lower, while their electrical conductivity is higher in comparison with SWCNTs [17,18]. In the work of Zhao et al., the use of highly dispersed PtSn/MWCNTs as anode catalyst of a direct ethanol fuel cell was investigated. It was found that MWCNTs as the support of PtSn bimetallic anode catalyst exhibited better performance compared to XC-72 carbon. Its higher electrocatalytic activity was attributed to the unique structure, better electric properties and lower organic impurities of MWCNTs [10].

Nevertheless, CNTs are insoluble and quite difficult to disperse in most solvents and polymers for their large molecules with thousands of carbon atoms in an aromatic delocalized system [19]. Additionally, CNTs, due to their relatively low surface area, lack sufficient binding sites for anchoring precursor metal ions or metal nanoparticles, leading to poor dispersion and aggregation of metal nanoparticles, especially at high metal loading conditions [6]. Therefore, the surface modification of CNTs with functional groups is the key for their further applications.

Among all the modification methods, surface oxidation is the most adopted one, due to the fact that it enables the removal of amorphous carbon from the non-activated MWCNTs [20] as well as makes MWCNTs opened at the end and terminal carbons for the insertion of metal carbon nanoparticles [21,22]. Considerable efforts have been made towards the modification of CNTs as catalyst supports in fuel cells. $H_2O_2$-oxidized MWCNTs provides PtRu with higher activity towards hydrogen oxidation reaction [23]. Li et al. have shown that HF treated MWCNTs supported Pt exhibited enhanced activity and stability for methanol oxidation [24]. KOH activation is also an effective route to improve the specific surface area and pore size distribution for CNTs [25], facilitating the access of the active phase during catalyst preparation, as well as enabling high catalyst dispersion.

The present work aims to investigate the KOH activating effect MWCNTs as Pt nanoparticles support for ORR. The surface functional groups and the structure of MWCNTs were characterized by the techniques of infrared and Raman spectroscopy. The structural properties of KOH-activated MWCNTs supported Pt were investigated by X-ray diffraction (XRD) and transmission electron microscopy (TEM) and their electrochemical performance was evaluated by the use of cyclic voltammetry (CV) and rotating disk electrode (RDE) voltammetry.

## 2. Experimental

### 2.1. MWCNTs treatment [12]

MWCNTs with diameters of 10–20 nm and purity of >95% (Shenzhen Nanotech. Co., Ltd., China) were adopted. The as-received MWCNTs were physically mixed with KOH powder at the KOH/MWCNTs mass ratio of 4/1. After drying at 110 °C for 12 h, the activation process was carried out at 700, 800, and 900 °C for 1 h at a heating rate of 5 °C min$^{-1}$ under N$_2$ flow (500 mL min$^{-1}$). Afterwards, the samples were washed with 5.0 mol L$^{-1}$ HCl for 30 min and filtered until there was no Cl$^-$ detected by 1.0 mol L$^{-1}$ AgNO$_3$.

The activated MWCNTs were obtained after drying at 110 °C in an oven for 12 h. The obtained samples are denoted as MWCNTs-700, MWCNTs-800 and MWCNTs-900, where 700, 800 and 900 are the corresponding activation temperature values in Celsius degree.

### 2.2. Pt/MWCNTs preparation

The 20 wt.% Pt/MWCNTs electrocatalysts were easily and fast prepared by a pulse-microwave assisted polyol method [26,27]. The primary steps of this synthesis process are given as follows: in a beaker, chloroplatinic acid, the starting precursor was well mixed with ethylene glycol (EG) in an ultrasonic bath, and then MWCNTs were added into the mixture. After the pH value of system was adjusted to more than 10 by the drop-wise addition of NaOH/EG, the well-dispersed slurry was obtained with stirring and ultrasonication for 30 min. Thereafter, the slurry was microwave-heated in the pulse form of 5 s-ON/5 s-OFF for several times. After re-acidification, the resulting black solid sample was filtered, washed and dried at 80 °C for 10 h in a vacuum oven. The as-prepared Pt/MWCNTs catalysts are denoted as Pt/MWCNTs, Pt/MWCNTs-700, Pt/MWCNTs-800, and Pt/MWCNTs-900.

### 2.3. Characterization of MWCNTs and Pt/MWCNTs

The Fourier transform infrared spectroscopic measurements were carried out on a Nicolet 5700 spectrometer (Thermo, USA). The Raman spectroscopic measurements were performed on a Renishaw Raman spectrometer (Renishaw Corp., UK) using a He/Ne laser with the wavelength of 514.5 nm. The XRD measurements were carried out on a D/Max-IIIA (Rigaku Co., Japan) using Cu Kα radiation ($\lambda = 0.15406$ nm), and operating at 40 kV and 40 mA. The $2\theta$ angular regions between 20 and 90° were explored at a scan rate of 5° min$^{-1}$ and the 62–72° angle range was finely scanned at 1° min$^{-1}$ in order to obtain the average Pt particle size precisely according to the Scherrer formula [28]. All electrochemical measurements were conducted on a PARSTAT 2273 instrument in a thermostat-controlled standard three-electrode cell at room temperature, adopting a saturated calomel electrode (SCE) and a platinum foil (1.0 cm × 1.0 cm) as the reference and the counter electrode, respectively. A glassy carbon (GC) disk electrode was used as the substrate for the electrocatalyst thin film in the electrochemical measurements. The thin film catalyst layer as the working electrode was prepared as follows: a mixture containing 5.0 mg electrocatalysts, 1.8 mL ethanol and 0.2 mL Nafion solution (5 wt.%) was dispersed in a ultrasonic bar for 10 min in order to obtain a well-dispersed ink. The catalyst ink was then quantitatively transferred onto the surface of the GC electrode by using a micropipette, and dried under infrared lamp to obtain a catalyst thin film. The Pt loading was 25.5 μg cm$^{-2}$ for each catalyst. An aqueous solution containing 0.5 mol L$^{-1}$ H$_2$SO$_4$ was used as electrolyte, which was deaerated with high-pure nitrogen gas. Rotating disk electrode (RDE) was carried out in an oxygen-saturated 0.5 mol L$^{-1}$ H$_2$SO$_4$ solution with a potential range from 1.0 to 0 V (vs. SCE) at a rotating speed of 2500 rpm and the scan rate was 5 mV s$^{-1}$.

## 3. Results and discussion

The types of the chemical groups on the surface of MWCNTs were characterized by Fourier transform infrared spectroscopy (FTIR) and the corresponding results are shown in Fig. 1. The band at 1631 cm$^{-1}$ is attributed to OH stretching vibration. The band at 1087 cm$^{-1}$ corresponds to C–O stretching vibration. From the FTIR spectrum, it is obvious that there are many oxygen-containing functional groups distributing on the surface of the activated MWCNTs. Compared to the case of the as-received MWCNTs, it can be deduced that MWCNTs have been successfully functionalized by
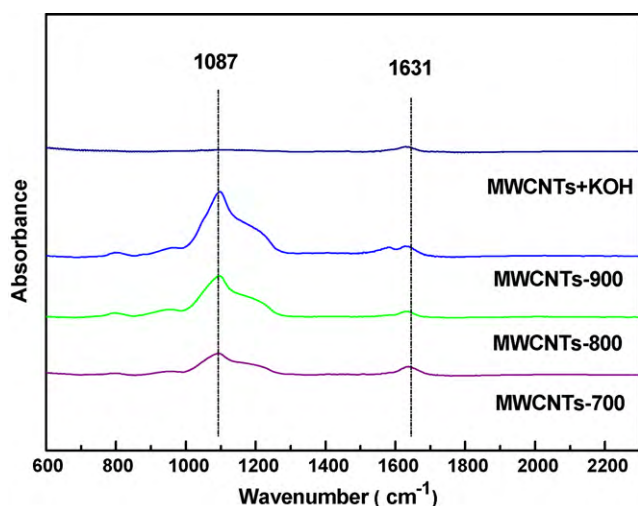
**Fig. 1.** FTIR spectra of MWCNTs activated by KOH at different temperatures and as-received.



**Fig. 2.** Raman spectra of MWCNTs activated by KOH at different temperatures and as-received.

KOH with the high temperature treatment. As the electrocatalyst support, the oxygen-containing groups on MWCNTs are of great interest in the preparation of supported catalysts because this could enhance the hydrophilicity of MWCNTs, which is helpful for the fine dispersion of metal atoms. At the same time, this could stabilize noble metal ions. The noble metal atoms are maintained on the outer surface of MWCNTs after reduction, which tend to coalescence, forming noble metal nanoparticles. These noble metal nanoparticles would be ultimately stabilized by a strong bonding interaction between the surrounding oxygen atoms of MWCNTs. According to this mechanism, the C–O and OH groups can act as glue to anchor the noble metal nanoparticles on the surface of MWCNTs [29–31].

From the Raman results as shown in Fig. 2, it can be clearly seen that the samples give similar Raman scattering patterns. The peak at 1352 cm$^{-1}$ is assigned to the disordered graphite (D-line). The peak at high frequency of ~1577 cm$^{-1}$ corresponds to a splitting of the E$_{2g}$ stretching mode of graphite and reflects the structural intensity of the sp$^2$-hybridized carbon atom, which denotes for G-line [32,33]. The intensity ratio between the D-line and G-line can
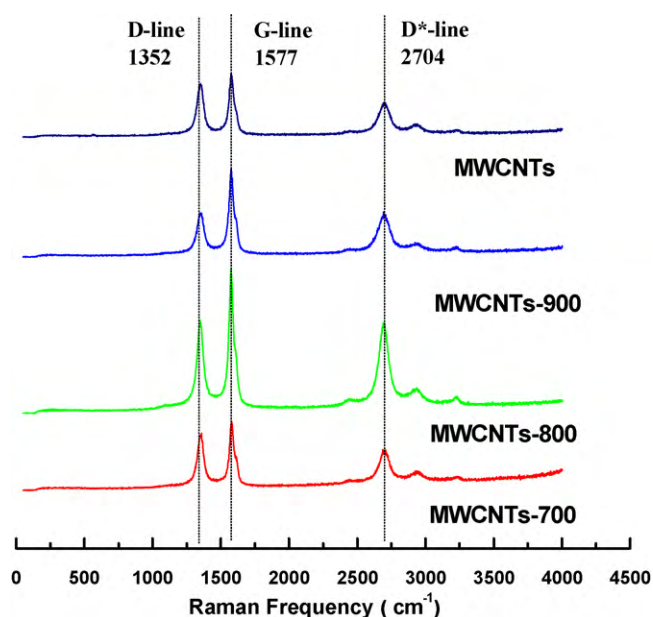
be used as an indicator for the extent of the modification or defect on CNTs [34]. Based on the Raman curves, it can be calculated that the intensity ratio of the D-line to G-line is 0.83, 0.64, 0.50 and 0.82 for MWCNTs-700, MWCNTs-800, MWCNTs-900, and MWCNTs as-received, respectively. Obviously, the treatment temperature is a key parameter. As the temperature increases, the graphitization degree of MWCNTs gets higher, which is a desirable property since the degree of graphitization is a key factor affecting the electrical conductivity and stability [35].

In order to investigate the chemical reaction process taking place in the activation of MWCNTs by KOH powder, thermalgravity (TG) was carried out under N$_2$ atmosphere. For the sake of reference, the as-received MWCNTs were also tested and the results are given in Fig. 3. As clearly seen, in the case of the as-received MWCNTs, there is a small weight loss in all the investigated temperature range, which could be attributed to the partial oxidization of
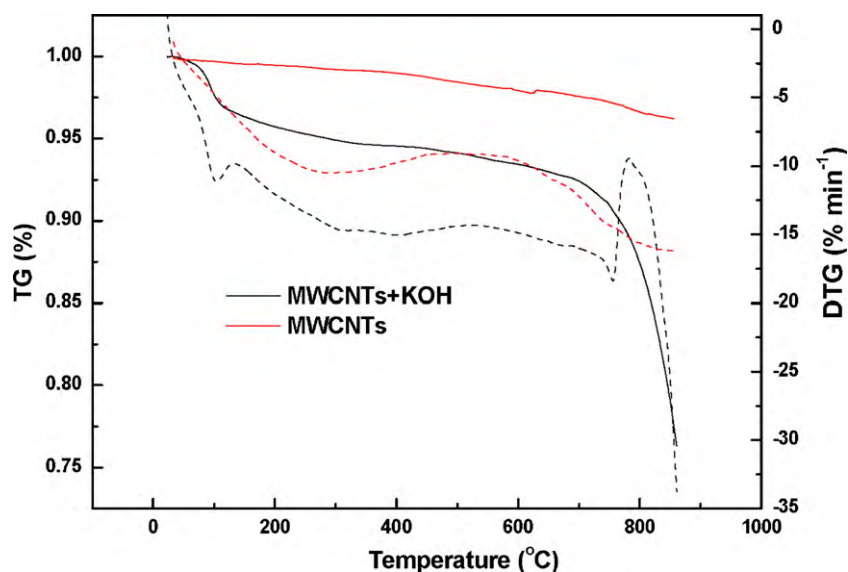


**Fig. 3.** TG and DTG results for MWCNTs and KOH reactions. The heating rate was 10 °C min$^{-1}$. The solid and dash line correspond to TG vs. temperature and DTG vs. temperature curves, respectively.

MWCNTs with the trace oxygen from the $N_2$ atmosphere or system leakage. In the case of MWCNTs + KOH, there is an obvious weight loss in the corresponding TG and differential-thermal gravity (DTG) curves from room temperature up to approximately 100 °C, which could be due to the water release in the sample. The more water in MWCNTs + KOH derives from the strong capability of KOH powder to absorb water. When the temperature increases up to 780 °C, MWCNTs can react chemically with KOH according to reactions (1) and (2) [36]:

$$4KOH + C \leftrightarrow 4K + CO_2 + H_2O \qquad (1)$$

$$6KOH + C \rightarrow 2K + 3H_2 + 2K_2CO_3 \qquad (2)$$
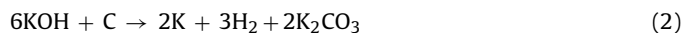
This indicates that MWCNTs can be activated by KOH at high temperatures through the chemical reaction between them. The produced gases are released from the system, thus leading to the weight loss.

In order to investigate the effect of KOH activation on MWCNTs properties, the treated MWCNTs were adopted as the support for the Pt catalysts in the present work, while in turn for the sake of comparison the as-received MWCNTs were also used as the supports. In Fig. 4 the XRD patterns of the as-prepared Pt/MWCNTs catalysts are presented. The diffraction peaks at 20–25° observed in all the investigated samples are attributed to the hexagonal graphite structure (0 0 2). Furthermore, all the samples show the typical characteristics of a crystalline Pt face centered cubic (fcc) structure. The diffraction peaks at $2\theta = 39.6$, 46.3, 67.4 and 81.6°
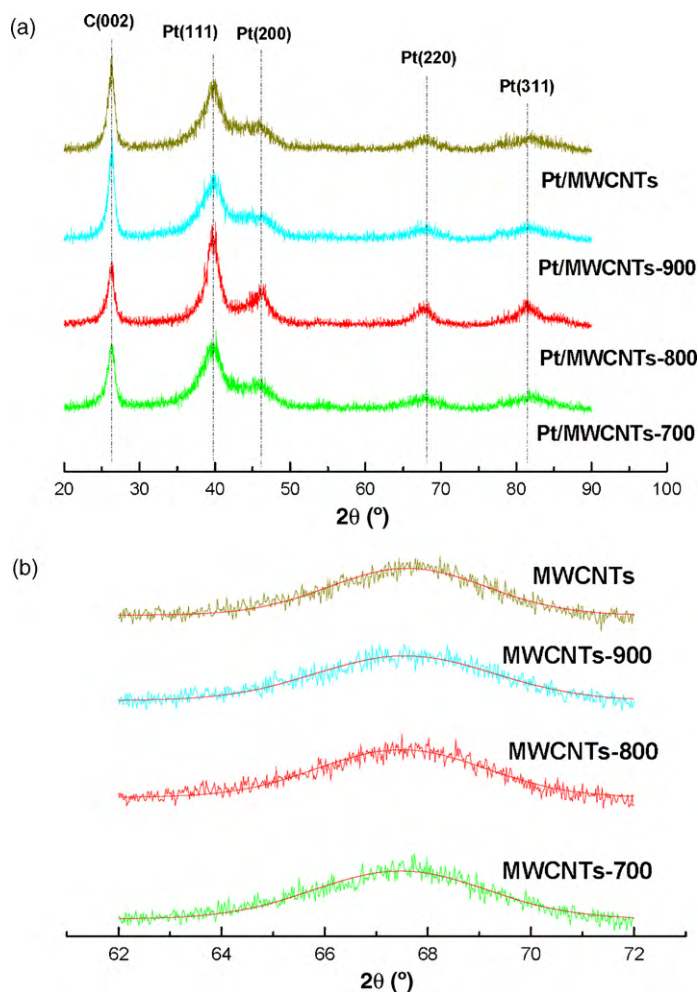
(a)

(b)

**Fig. 4.** XRD patterns of Pt catalysts supported on activated and as-received MWCNTs and their corresponding Pt (2 2 0) peaks.
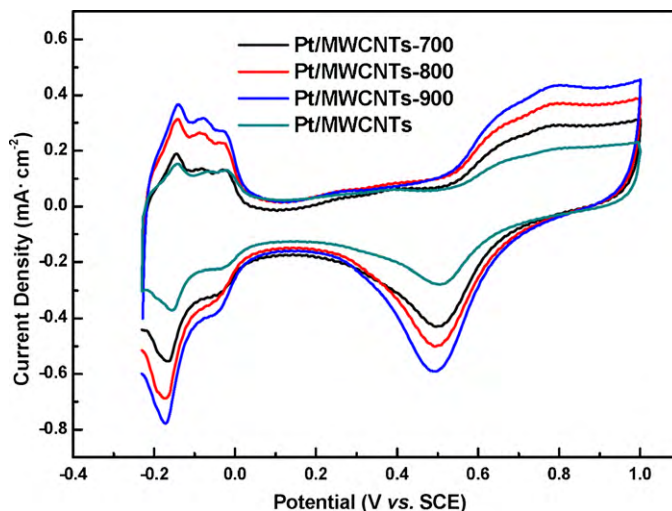
**Fig. 5.** Cyclic voltammetry curves of the as-prepared Pt/MWCNTs-700, Pt/MWCNTs-800, Pt/MWCNTs-900, and Pt/MWCNTs catalysts in 0.5 mol L$^{-1}$ $H_2SO_4$ at room temperature. Scan rate: 20 mV s$^{-1}$.

are assigned to the Pt (1 1 1), Pt (2 0 0), Pt (2 2 0) and Pt (3 1 1) facets, respectively. The fitted (2 2 0) plane was used to calculate the average Pt particle size according to the Scherrer formula [28]. The respective average particle size (d) of Pt/MWCNTs-700, Pt/MWCNTs-800, Pt/MWCNTs-900, and Pt/MWCNTs is 2.9, 2.8, 2.9, and 3.2 nm.

The cyclic voltammetry (CV) curves of all the samples in the deaerated 0.5 mol L$^{-1}$ $H_2SO_4$ by adopting the thin porous coating microelectrode technique with a catalyst loading of 25.5 μg Pt cm$^{-2}$, are shown in Fig. 5. From the integrated charge in the hydrogen adsorptions peak areas in the CV curves and the Pt poly-crystallite hydrogen adsorption constant 210 μC cm$^{-2}$ Pt, the electrochemical surface area ($S_{ESA}$), for each catalyst can be calculated using the following equation [37,38]:

$$S_{ESA}[m^2 Pt/gPt] = \frac{charge[\mu C\,cm^{-2}]}{\{210[\mu C\,cm^{-2}Pt] \times Pt\,loading[mg\,cm^{-2}]\} \times 10^{-1}} \qquad (3)$$

The $S_{ESA}$ value for Pt/MWCNTs-700, Pt/MWCNTs-800, Pt/MWCNTs-900, and Pt/MWCNTs is 25, 50, 60, and 20 m$^2$ g$^{-1}$, respectively. Clearly, after KOH activation, the electrochemical surface area increases. It is worthy to be noticed that the $S_{ESA}$ of Pt/MWCNTs-900 is two times higher than that of Pt/MWCNTs. In the case of the same Pt loading, the higher the electrochemical surface area is, the higher Pt utilization efficiency will be. This indicates that KOH activation helps the interaction of the precursor solution with the MWCNTs surface during the catalysts synthesis process, resulting in good catalyst dispersion as shown in the TEM images given in Fig. 6. This could be attributed to the increased surface area and pore size distribution by KOH activation [25]. Moreover, according to the FTIR results, the MWCNTs surface has been successfully decorated with the oxygen-containing groups. As a consequence the hydrophilicity of the MWCNTs will be increased, making the surface more accessible to the aqueous solution of the metal precursor during impregnation.

For the further electrochemical characterization, the corresponding activity for ORR of all the samples was evaluated in an $O_2$-saturated 0.5 mol L$^{-1}$ $H_2SO_4$ solution by using the technique of RDE voltammetry. From Fig. 7(a) it is obvious that KOH activation of MWCNTs can enhance Pt/MWCNTs' activity towards ORR. This improvement increases along with the activation temperature increment. Finally, the ORR onset potential in all cases corresponds approximately to 0.70 V (vs. SCE) (Fig. 7(b)).
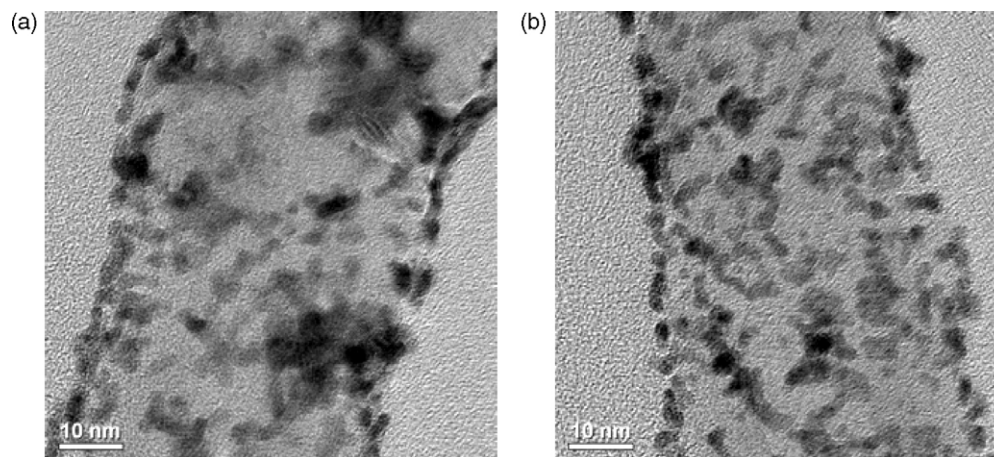
**Fig. 6.** TEM images of the as-prepared Pt/MWCNTs-900 (a) and Pt/MWCNTs (b) catalysts.
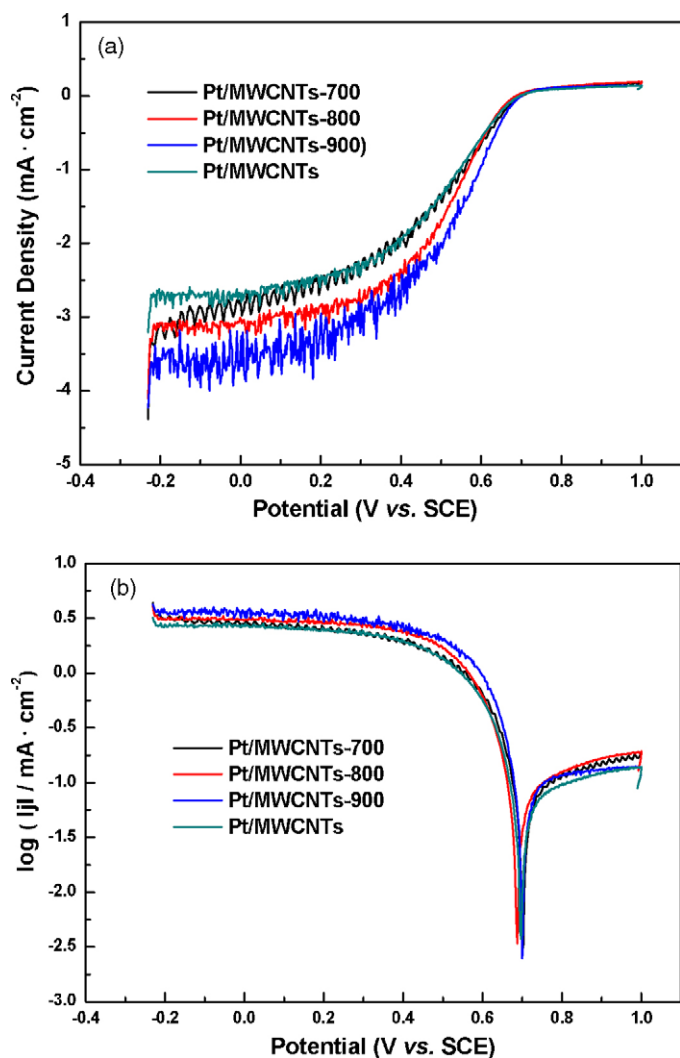


**Fig. 7.** (a) Polarization curves of oxygen reduction reaction on Pt/MWCNTs-700, Pt/MWCNTs-800, Pt/MWCNTs-900, and Pt/MWCNTs in $O_2$-saturated 0.5 mol L$^{-1}$ H$_2$SO$_4$ solution at a scan rate of 5 mV s$^{-1}$; rotation speed 2500 rpm. (b) The corresponding Tafel plots for ORR on all the catalysts.

The mass activity (MA) of a Pt-based catalyst is the corresponding net kinetic current ($i_{kin}$) of ORR at a given potential divided by the mass of Pt. The $i_{kin}$ can be obtained by using the following equation:

$$MA = I_{kin} = \frac{i_{lim}i_{obs}}{i_{lim} - i_{obs}} \tag{4}$$

where $i_{lim}$ is the limiting current and $i_{obs}$ is the observed current value. Based on the experimental results shown in Fig. 7 and Eq. (4), it can be found that Pt/MWCNTs-900 has the highest mass activity of 79.2 mA mg$^{-1}$, while the corresponding values for Pt/MWCNTs-700, Pt/MWCNTs-800, and Pt/MWCNTs are 56.3, 66.9 and 52.3 mA mg$^{-1}$ at a given potential of 0.5 V (vs. SCE). The highest performance of Pt/MWCNTs-900 could be attributed to the better dispersion of Pt nanoparticles on the surface of MWCNTs. This results from the higher surface area and the wider pore size distribution of MWCNTs activated by KOH at higher temperature [25].

## 4. Conclusions

Based on the experimental results of the present work the surface of MWCNTs has been successfully functionalized with oxygen-containing groups after activation by KOH at higher temperature. This is favorable for the good dispersion of Pt nanoparticles on them. From the electrochemical performance point of view, the electrochemical active area of Pt/MWCNTs-900 is increased twofold compared to Pt/MWCNTs, leading to higher oxygen reduction reaction activity. At a given potential of 0.5 V (vs. SCE) the mass activity of Pt/MWCNTs-900 equals to 79.2 mA mg$^{-1}$, while the corresponding values for Pt/MWCNTs-700, Pt/MWCNTs-800 and Pt/MWCNTs are 56.3, 66.9 and 52.3 mA mg$^{-1}$. It can be concluded that KOH activation is an effective way to decorate MWCNTs' surface with oxygen-containing groups and provide MWCNTs with high surface area, making them more suitable as support materials of electrocatalysts.

# References

[1] A.L.W. Vielstich, H. Gasteiger (Eds.), Handbook of Fuel Cells: Fundamentals, Technology, Applications, Wiley, 2003.

[2] S. Song, P. Tsiakaras, Appl. Catal. B: Environ. 63 (2006) 187–193.

[3] X. Yu, S. Ye, J. Power Sources 172 (2007) 133–144.

[4] X. Yu, S. Ye, J. Power Sources 172 (2007) 145–154.

[5] H.A. Gasteiger, S.S. Kocha, B. Sompalli, F.T. Wagner, Appl. Catal. B: Environ. 56 (2005) 9–35.

[6] E. Antolini, Appl. Catal. B: Environ. 88 (2009) 1–24.

[7] W. Li, C. Liang, J. Qiu, W. Zhou, H. Han, Z. Wei, G. Sun, Q. Xin, Carbon 40 (2002) 791–794.

[8] P. Serp, M. Corrias, P. Kalck, Appl. Catal. A: Gen. 253 (2003) 337–358.

[9] C. Yang, X. Hu, D. Wang, C. Dai, L. Zhang, H. Jin, S. Agathopoulos, J. Power Sources 160 (2006) 187–193.

[10] X. Zhao, W. Li, L. Jiang, W. Zhou, Q. Xin, B. Yi, G. Sun, Carbon 42 (2004) 3263–3265.

[11] A.C. Dillon, K.M. Jones, T.A. Bekkedahl, C.H. Kiang, D.S. Bethune, M.J. Heben, Nature 386 (1997) 377–379.

[12] S.M. Lee, S.C. Lee, J.H. Jung, H.J. Kim, Chem. Phys. Lett. 416 (2005) 251–255.

[13] Y. Ye, C.C. Ahn, C. Witham, B. Fultz, J. Liu, A.G. Rinzler, D. Colbert, K.A. Smith, R.E. Smalley, Appl. Phys. Lett. 74 (1999) 2307–2309.

[14] A.G. Rinzler, J.H. Hafner, P. Nikolaev, L. Lou, S.G. Kim, D. Tomanek, P. Nordlander, D.T. Colbert, R.E. Smalley, Science 269 (1995) 1550–1553.

[15] C. Niu, E.K. Sichel, R. Hoch, D. Moy, H. Tennent, Appl. Phys. Lett. 70 (1997) 1480–1482.

[16] H.-F. Cui, J.-S. Ye, W.-D. Zhang, J. Wang, F.-S. Sheu, J. Electroanal. Chem. 577 (2005) 295–302.

[17] Y. Shao, G. Yin, J. Wang, Y. Gao, P. Shi, J. Power Sources 161 (2006) 47–53.

[18] C. Wang, M. Waje, X. Wang, J.M. Tang, R.C. Haddon, Y. Yan, Nano Lett. 4 (2004) 345–348.

[19] J. Qiu, G.J. Wang, Appl. Surf. Sci. 254 (2008) 5691–5694.

[20] T.W. Ebbesen, Adv. Mater. 8 (1996) 155–157.

[21] J. Chen, M.A. Hamon, H. Hu, Y. Chen, A.M. Rao, P.C. Eklund, R.C. Haddon, Science 282 (1998) 95–98.

[22] T.W. Ebbesen, P.M. Ajayan, H. Hiura, K. Tanigaki, Nature 367 (1994) 519–1519.

[23] Y. Liang, H. Zhang, B. Yi, Z. Zhang, Z. Tan, Carbon 43 (2005) 3144–3152.

[24] Y. Li, F.P. Hu, X. Wang, P.K. Shen, Electrochem. Commun. 10 (2008) 1101–1104.

[25] J.J. Niu, J.N. Wang, Y. Jiang, L.F. Su, J. Ma, Micropor. Mesopor. Mater. 100 (2007) 1–5.

[26] S. Song, Y. Wang, P.K. Shen, J. Power Sources 170 (2007) 46–49.

[27] S. Song, Y. Wang, P. Tsiakaras, P.K. Shen, Appl. Catal. B: Environ. 78 (2008) 381–387.

[28] V. Radmilovic, H.A. Gasteiger, P.N. Ross, J. Catal. 154 (1995) 98–106.

[29] X.L. Li, T.J. Lou, X.M. Sun, Y.D. Li, Inorg. Chem. 43 (2004) 5442–5449.

[30] W. Shen, Y. Zhu, X. Dong, J. Gu, J. Shi, Chem. Lett. 34 (2005) 840–841.

[31] C. Xu, L. Cheng, P. Shen, Y. Liu, Electrochem. Commun. 9 (2007) 997–1001.

[32] T. Belin, F. Epron, Mater. Sci. Eng. B: Solid-State Mater. Adv. Technol. 119 (2005) 105–118.

[33] M.S. Dresselhaus, G. Dresselhaus, R. Saito, A. Jorio, Phys. Rep. 409 (2005) 47–99.

[34] Z.Q. Tian, S.P. Jiang, Y.M. Liang, P.K. Shen, J. Phys. Chem. B 110 (2006) 5343–5350.

[35] P.V. Shanahan, L. Xu, C. Liang, M. Waje, S. Dai, Y.S. Yan, J. Power Sources 185 (2008) 423–427.

[36] M.A. Lillo-Rodenas, D. Cazorla-Amoros, A. Linares-Solano, Carbon 41 (2003) 267–275.

[37] W. Li, W. Zhou, H. Li, Z. Zhou, B. Zhou, G. Sun, Q. Xin, Electrochim. Acta 49 (2004) 1045–1055.

[38] G. Tamizhmani, J.P. Dodelet, D. Guay, J. Electrochem. Soc. 143 (1996) 18–23.